ELSEVIER

Contents lists available at ScienceDirect

# Chemical Engineering Journal

journal homepage: www.elsevier.com/locate/cej





# Sunlight-boosted recovery of precious metal ions from E-waste using tannin-grafted mesoporous silica

Jeonga Kim<sup>a</sup>, Kimoon Lee<sup>a</sup>, Cafer T. Yavuz<sup>b,c,d</sup>, Yoon Sung Nam<sup>a,e,\*</sup>

- <sup>a</sup> Department of Materials Science and Engineering, Korea Advanced Institute of Science and Technology, 291 Daehak-ro Yuseong-gu, Daejeon 34141, Republic of Korea <sup>b</sup> Oxide & Organic Nanomaterials for Energy & Environment (ONE) Laboratory, Physical Science & Engineering (PSE), King Abdullah University of Science and
- Technology (KAUST), Thuwal 23955, Saudi Arabia
  <sup>c</sup> Advanced Membranes & Porous Materials (AMPM) Center, Physical Science & Engineering (PSE), King Abdullah University of Science and Technology (KAUST), Thuwal 23955, Saudi Arabia
- d KAUST Catalysis Center (KCC), Physical Science & Engineering (PSE), King Abdullah University of Science and Technology (KAUST), Thuwal 23955, Saudi Arabia
- e Department of Biological Sciences, Korea Advanced Institute of Science and Technology, 291 Daehak-ro Yuseong-gu, Daejeon 34141, Republic of Korea

#### ARTICLE INFO

# Keywords: Precious metal recovery Metal ion adsorption Tannin Sunlight-boosted reduction Plasmonic enhancement

#### ABSTRACT

The escalating demand and dwindling reserves of precious metals request efficient recycling techniques from electron waste. Addressing this need, we introduce a new method utilizing tannin-grafted mesoporous silica for the sunlight-boosted recovery of precious metals. Our strategy leverages the inherent photoreactivity of tannins, enabling metal–ligand complexation and plasmonic enhancement of chemical reduction. The result is a marked increase in the adsorption capacity and the high selectivity towards precious metal ions in electronic waste. Our robust covalent bonding approach concentrated tannic acids onto silica at a high density (500,000 per square micrometer), which significantly boosted the adsorption of gold ions up to an 11-fold increase, even amidst a mixture of nine other metal species. Impressively, we achieved a maximum adsorption capacity of 68.4 mmol per gram, equivalent to 13.4 g of gold per gram of adsorbent. Also, the adsorption rates for platinum and palladium ions were enhanced by 2.6 and 3.0 times, respectively. The underlying mechanism includes the visible-light-driven plasmonic hot electron transfer that affords nearly perfect selectivity for gold ions (approximately 99%). These findings not only advance the field of metal recovery from electronic waste but also offer an environmentally benign and cost-effective solution that harnesses renewable solar energy.

# 1. Introduction

The utility of precious metals in optical, electrical, and catalytic applications is well established, yet their finite and dispersed nature reserves are insufficient for the burgeoning global demand [1]. This shortage brings attention to urban mining, especially the recycling of metals from secondary sources such as electronic waste (E-waste) to foster sustainable industrial progress and economic growth [2]. The conventional approach of precious metal leaching from E-waste involves hydrometallurgy – dismantling to remove non-metallic components, fragmentation, and treatment with an acidic solution (pH 1–3) including chlorine - yielding a complex mixture of chloro-metal ions [1,2]. The resultant leachate contains base and earth-abundant elements like Co, Ni, Cu, Fe, Al, and Zn in addition to precious metals, presenting an ongoing challenge for selective reclamation of precious metals.

Moreover, the variable and low concentrations of precious metals across different E-waste streams further complicate their recovery. Specifically, it is essential to effectively operate within wide concentration ranges such as those of Au (7–350 ppm), Pt (5–33 ppm), and Pd (4–210 ppm) found in E-waste, enabling selective separation and recovery of precious metals (Table S1). While several separation strategies are employed thereafter, including adsorption, solvent extraction, and ion exchange, they often result in incomplete metal recovery, generate secondary waste, and incur high costs [3,4]. Among them, adsorption is favored owing to its operational simplicity and predictability [5]. Various adsorbents have been attempted to incorporate functional moieties of nitrogen, sulfur, and oxygen atoms with great binding affinity for precious metal ions, including porous organic polymers, modified polysaccharides, chelating resins, and porous silica [6–18]. However, metal adsorption technologies still need to be more efficient, selective,

E-mail address: yoonsung@kaist.ac.kr (Y.S. Nam).

 $<sup>^{\</sup>ast}$  Corresponding author.

environment-friendly, and cost-effective for practical applications. To date, no adsorbent has demonstrated effectiveness across the wide concentration spectrum of target metal ions, from parts per million to substantial levels [19,20]. An ideal adsorbent would, therefore, combine a high capacity for precious metals with versatility across a wide range of metal ion concentrations.

Polyphenols, due to their phenolic hydroxyl groups, have proven to be effective in chelating metal ions, mitigating reactive oxygen species, and forming adhesive coatings at an economical cost [21-31]. Our previous investigations have particularly highlighted tannic acid (TA), a naturally occurring polyphenol, as a promising agent when physically applied to porous polymer microspheres, thus advancing the prospects for eco-friendly metal recycling [32]. It has been demonstrated that the photooxidation process enhances TA's adsorptive capability by utilizing its  $\pi$ -conjugation structure to harness ultraviolet (UV) light, substantially increasing the adsorption capacity for Au ions from 0.266 to 1.635 mmol g<sup>-1</sup> after irradiation. Nevertheless, when compared to other adsorbents detailed in Table S2, TA's maximum Au adsorption capacity appears modest. Certain adsorbents have demonstrated capacities exceeding 5 mmol  $g^{-1}$  for Au ions, surpassing their own weight, underlining the need for further optimization of TA-based adsorption systems.

Our literature review has led us to hypothesize that the low adsorption capacity of TA-deposited adsorbents may stem from the weak hydrogen bonds that anchor TA to the substrate, resulting in a low density of TA and the dissociation of both TA and captured Au ions. Prior experiments have consistently shown detachment of Au nanoparticles (AuNPs) from the polyphenol-based surface [32]. To address this, we propose enhancing the chemical stability and density of TA grafting onto substrates, critical in refining adsorption efficiency for precious metals, particularly amidst the competitive binding of various metal ions in E-waste. Furthermore, exploring the application of photochemical adsorption processes to other precious metals such as Pt and Pd, present in E-waste items such as printed circuit boards and mobile devices, is warranted. This exploration could advance the development of more selective and efficient recycling methodologies for valuable metals.

In this work, we investigated the robust covalent grafting of TA onto highly mesoporous silica particles, aiming to photochemically boost the selective capture of Au, Pt, and Pd ions from a complex mixture of metal ions typically found in E-waste. Utilizing mesoporous silica as a support combines stability and eco-friendliness with minimal optical interference, onto which TA was functionalized. This apporoach facilitated the stable and dense grafting of TA, enriching the surface with gallol and catechol groups necessary for biding and reducing precious metal ions. Simulated sunlight was employed to induce TA-mediated electron transfer to the metal ions, facilitating their efficient reduction. In addition, the covalent grafting of TA onto silica was instrumental in onsurface nucleation and growth of metal nanostructures, generating plasmonic hot electrons to selectively reduce precious metal ions, thus enhancing the adsorption capacity. For our adsorption experiments, an aqueous model solution mimicking E-waste, containing nine different metal ion species across various concentrations. After adsorption, metalloaded TA-grafted silica particles underwent desorption processes for metal recovery.

# 2. Experimental section

# 2.1. Materials

TA, 3-aminopropyltrimethoxysilane (APTMS), 50 wt-% glutaraldehyde, anhydrous toluene, aluminum chloride hexahydrate (AlCl<sub>3</sub>·6H<sub>2</sub>O), gold (III) chloride (AuCl<sub>3</sub>), cobalt(II) chloride hexahydrate (CoCl<sub>2</sub>·6H<sub>2</sub>O), palladium (II) chloride (PdCl<sub>2</sub>), nickel (II) chloride hexahydrate (NiCl<sub>2</sub>·6H<sub>2</sub>O), platinum (IV) chloride (PtCl<sub>4</sub>), zinc chloride (ZnCl<sub>2</sub>), copper (II) chloride dehydrate (CuCl<sub>2</sub>·2H<sub>2</sub>O), iron (III) chloride hexahydrate (FeCl<sub>3</sub>·6H<sub>2</sub>O), thiourea, and sodium borohydride (NaBH<sub>4</sub>)

were purchased from Sigma-Aldrich (St. Louis, MO, USA). Porous silica particles (p-silica) were obtained from EastHill Corporation (Suwon, Republic of Korea). Hydrochloric acid (HCl) and nitric acid (HNO $_3$ ) were purchased from Thermo Fisher Scientific (Waltham, MA, USA). Ethanol (94.5 %) was purchased from Daejung Chemicals (Siheung, Republic of Korea).

# 2.2. Amine-functionalized porous silica particles

Primary amine-functionalized silica particles (p-silica-NH $_2$ ) were prepared using APTMS according to a previous report with modification [33–35]. Porous silica particles (2 g) were immersed in anhydrous toluene (100 mL) with magnetic stirring at 600 rpm while refluxed at 120 °C for 10 min under a nitrogen atmosphere. APTMS (2 mL) was added using a syringe needle while mixed with magnetic stirring at 400 rpm and refluxed at 120 °C for 24 h under the same atmosphere. Aminefunctionalized particles were separated and then repeatedly washed by centrifugation (1000  $\times$  g) with subsequent ultrasonic dispersion for 20 min. The washed amine-functionalized silica particles were dried in a vacuum.

#### 2.3. Surface functionalization of porous silica particles with TA

TA-grafted silica particles (p-silica-TA) were prepared with glutaraldehyde as a crosslinking agent using a modified method described previously [36,37]. The dried amine-functionalized silica particles (100 mg) were dispersed in deionized water (8 mL) using vortex mixing and sonication for 20 min. The dispersion was transferred to a flask and stirred at 600 rpm and 37 °C, resulting in the dispersion of the silica particles (10 mg mL $^{-1}$ ). The dispersion was blended with TA solution (10 mg mL $^{-1}$ ) in deionized water, 2 mL) at 600 rpm and 37 °C. Glutaraldehyde (0.32 mL, 50 wt-%) was put into the mixture and magnetically blended at 600 rpm at 37 °C for 24 h. The TA-grafted silica particles were repeatedly washed using centrifugation (1000  $\times$  g) with subsequent ultrasonic dispersion for 10 min, followed by vacuum drying.

# 2.4. Multi-metal adsorption

Multiple metal chlorides (AuCl<sub>3</sub>, PtCl<sub>4</sub>, PdCl<sub>2</sub>, AlCl<sub>3</sub>, CuCl<sub>2</sub>, FeCl<sub>3</sub>, NiCl<sub>2</sub>, ZnCl<sub>2</sub>, and CoCl<sub>2</sub>) were used as a simulated E-waste solution to investigate multi-metal adsorption characteristics. Dispersions (10 mg mL<sup>-1</sup>) of pristine *p*-silica, *p*-silica-NH<sub>2</sub>, and *p*-silica-TA were prepared in deionized water using vortex mixing and sonication for 20 min. Mixtures of the metal chlorides with p-silica, p-silica-NH2, and p-silica-TA dispersions were prepared to make 0.1, 1, and 2 mM in 0.1 M HCl of the metal chlorides and 0.5 mg mL<sup>-1</sup> of the particles. The suspensions were magnetically stirred at 300 rpm and 25 °C for 3 h with and without light irradiation. AM 1.5-simulated sunlight (Asahi Spectra HAL-320, Torrance, CA, USA) was exposed to the blends. The particles were recovered by centrifugation (1000  $\times$  g). The supernatants were used for quantitative analysis using inductively coupled plasma optical emission spectrometry (ICP-OES, Agilent ICP-OES 5110, Santa Clara, CA, USA) after filtering with a syringe filter (a pore diameter of  $0.2 \mu m$ ). The collected particles were dried after repeated washing by centrifugation (1000 ×

# 2.5. Adsorption isotherm

The dispersions (10 mg mL $^{-1}$ ) of pristine  $p\text{-silica}, p\text{-silica-NH}_2,$  and p-silica-TA particles in deionized water were mixed with an aqueous solution of AuCl $_3$ , PtCl $_4$ , and PdCl $_2$  to make multiple metal concentrations (0.25, 0.5, 1, 1.5, 2 and 3 mM in 0.1 M HCl) and 0.5 mg mL $^{-1}$  of the particles. The suspensions were stirred for 3 h at 300 rpm and 25 °C with and without light. The particles were recovered by centrifugation (1000  $\times$  g). The supernatants were used for quantitative analysis using ICPOES after filtering with the syringe filter. The collected particles were

dried after repeated washing by centrifugation (1000  $\times$  g).

#### 2.6. Metal desorption

The desorption of metal ions from p-silica-TA was performed with a mixture of HCl and HNO $_3$  (HCl:HNO $_3=3:1~v/v)$  or an acidic thiourea solution (1 M thiourea in 1 M HCl). The dried p-silica-TA obtained after the exposure to metal ions, denoted as 'M-p-silica-TA,' was immersed in the mixture of HCl and HNO $_3$  or the acidic thiourea solution (0.5 mg mL $^{-1}$ ) and stirred for 3 h at 25 °C. M-p-silica-TA particles were recovered by centrifugation (1000  $\times$  g), and the supernatants were used for quantitative analysis using ICP-OES after filtering with the syringe filter. The collected particles were dried in a vacuum after repeated washing by centrifugation (1000  $\times$  g).

# 2.7. Characterizations

A nitrogen gas adsorption analyzer (Micromeritics 3Flex, Norcross, GA, USA) was used to determine the surface area and pore size distributions of p-silica, p-silica-NH<sub>2</sub>, and p-silica-TA. The specific surface area and average pore width were determined using the Brunauer-Emmett-Teller isotherm and Barrett, Joyner, and Halenda method, respectively. A UV-visible-NIR spectrophotometer (Shimadzu SolidSpec-3700, Kyoto, Japan) was used to measure the absorbance of psilica, p-silica-NH<sub>2</sub>, and p-silica-TA dispersed in deionized water with an integrating sphere. Field emission scanning electron microscopy (SEM, Hitachi SU5000, Tokyo, Japan) and field-emission transmission electron microscopy (TEM, FEI Company Tecnai F20, Hillsboro, Oregon, USA) analyses were performed to explore morphologies of p-silica, p-silica-NH<sub>2</sub>, and p-silica-TA before and after the adsorption of metal ions with backscattered electrons (BSE), energy-dispersive X-ray spectroscopy (EDS), high-angle annular dark-field (HAADF) imaging, and scanning TEM (STEM) analysis. Fourier-transform infrared spectroscopy (FT-IR, Jasco FT/IR-6100, Tokyo, Japan) was used to analyze the chemical functionality of p-silica-TA and p-silica-TA before and after the adsorption of metal ions. X-ray photoelectron spectroscopy (XPS, Thermo VG Scientific, Waltham, MA, USA) was used at 4 kV and 5  $\mu$ A to analyze the surface chemistry of p-silica-TA and M-p-silica-TA. Thermogravimetric analysis (TGA, Netzsch TG209 F1 Libra, Selb, Germany) was conducted for quantitative analysis of TA grafting from 25 to 800 °C at a heating rate of 10 °C min<sup>-1</sup>. High-resolution X-ray powder diffraction (XRD, Rigaku SmartLab, Tokyo, Japan) was used at 45 kV and 200 mA to detect metals on M-p-silica-TA.

# 3. Results and discussion

# 3.1. Ta-grafted mesoporous silica particles

Mesoporous silica particles, referred to as 'p-silica,' were functionalized with primary amine groups through silanization using 3-aminopropyltrimethoxysilane (APTMS) (step 1). Specifically, APTMS underwent hydrolysis, replacing methoxy groups with hydroxyl groups, followed by condensation to form siloxane bonds on the *p*-silica surface. TA was then covalently grafted to the amine-functionalized silica particles, denoted by 'p-silica-NH2,' using glutaraldehyde as a bifunctional coupling agent to form imine and acetal bonds (step 2). This process yielded TA-grafted silica particles, denoted by 'p-silica-TA,' as illustrated in Fig. 1A. Despite the chemical modifications, the mesoporous and rough structural features were maintained, as confirmed by transmission electron microscopy (TEM) and scanning electron microscopy (SEM) analyses (Fig. 1B, 1C, and Supplementary Fig. S1A-H). However, the surface area and average pore width of mesoporous p-silica-TA were significantly reduced to 160.84 m<sup>2</sup> g<sup>-1</sup> and 9.79 nm, respectively, a decrease from pristine p-silica's 310.48 m<sup>2</sup> g<sup>-1</sup> and 15.79 nm (Fig. 2A) and Table S2). This reduction seems to be caused by the bulky molecular structure of TA. The p-silica-TA particles had an average particle

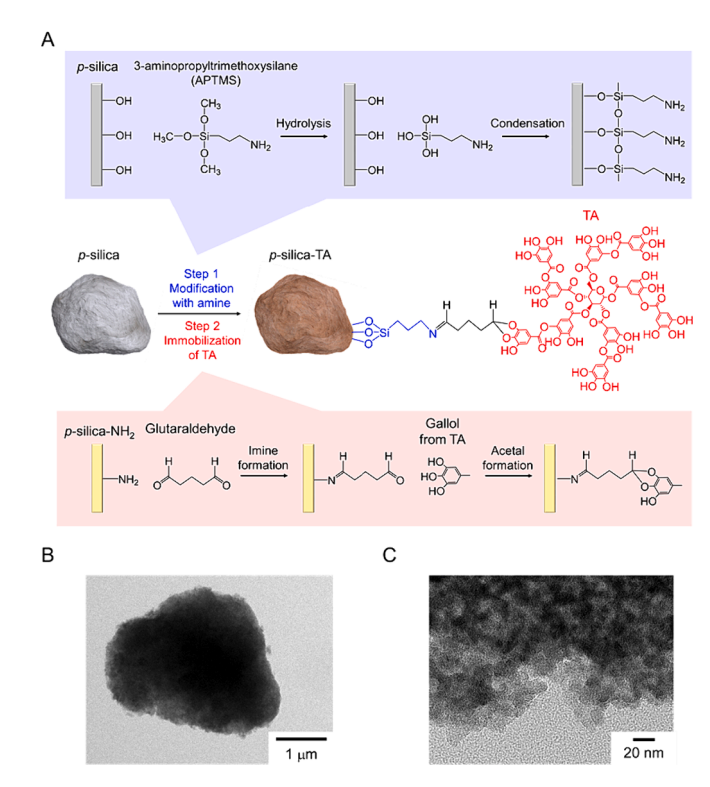


**Fig. 1.** (A) Schematic explanation for the fabrication of p-silica-TA. The internal and external surfaces of porous silica particles were modified with APTMS to introduce primary amines, followed by TA grafting using glutaral-dehyde as a coupling agent. TEM images of p-silica-TA at low (B) and high (C) magnifications.

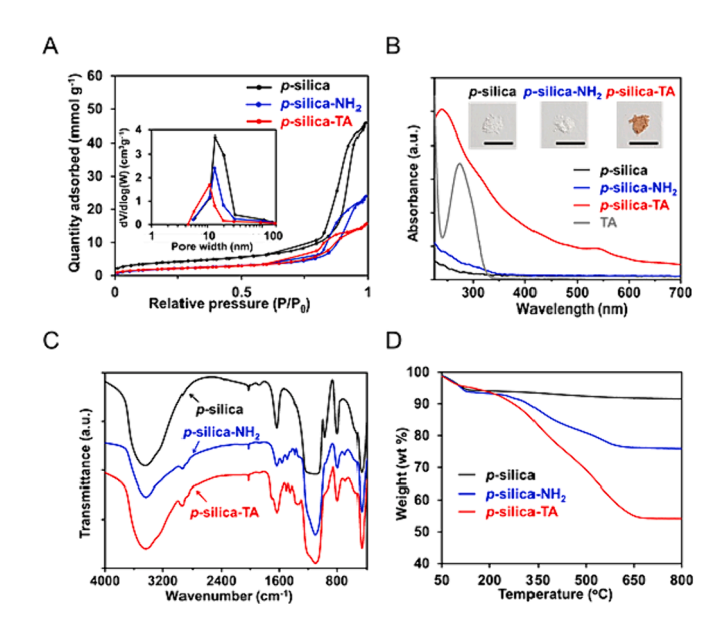


**Fig. 2.** (A) Brunauer-Emmett-Teller (BET) isotherm plots of  $N_2$  gas adsorption for p-silica, p-silica- $NH_2$ , and p-silica-TA (inset: pore volume distribution for p-silica and p-silica-TA exhibiting that the pore volume V is mostly derived from the mesopores in width W. UV–vis absorption spectra (B), FT-IR spectra (C), and TGA thermograms (D) of p-silica, p-silica- $NH_2$ , and p-silica-TA. The absorption spectra were obtained using the particle dispersion in deionized water using an integrating sphere (inset: optical photographs for powders of each particle, scale bar: 1 cm). A TA solution was included for comparison.

diameter of  $3.14\pm1.20~\mu m$ , appropriate for adsorption applications due to the balance between facile dispersion in solution and ease of separation (Fig. S1I). Spectral analysis indicated that p-silica-TA exhibited a broader absorption spectrum than TA alone, presumably due to the high-density grafting leading to aggregation within the pores, imparting a brownish hue to p-silica-TA (Fig. 2B). This extended light absorption spectrum could enhance photochemical activation by natural sunlight, a potential advantage for metal recovery applications.

Fourier-transform infrared spectroscopy (FT-IR) analysis verified the successful silanization and TA coupling (Fig. 2C). Specifically, the FT-IR spectrum of p-silica-NH $_2$  displayed characteristic N–H bending and C–H stretching peaks at 1580 and 2924–2850 cm<sup>-1</sup>, respectively. Peaks correlating to Si-O-Si bending and stretching were also observed at 467, 797. and  $1086 \text{ cm}^{-1}$  [38–40]. For *p*-silica-TA, peaks at 1690 and 1300 cm<sup>-</sup>1 confirmed the presence of imine and acetal functionalities, indicative of Schiff's base and acetal formation during the TA coupling process [41,42]. TA presence was also confirmed by C = O stretching and phenolic O-H bending peaks at 1710 and 1380-1310 cm<sup>-1</sup>, respectively [38,39,42]. X-ray photoelectron spectroscopy (XPS) analysis further corroborated the surface modification. Survey spectra exhibited N1s and C1s peaks for p-silica-NH<sub>2</sub>, with an increased C1s peak intensity for psilica-TA (Fig. S2A). The detailed spectral deconvolution of the C1s, O1s, N1s, and Si2p regions revealed signatures of organosilane and amine on p-silica-NH2 and imine, acetal, alcohol, and ester on p-silica-TA, confirming the conjugation of TA to NH2-functionalized silica via glutaraldehyde (Fig. S2B-E). Thermogravimetric analysis (TGA) quantified the TA grafting on p-silica-TA, revealing a grafting density approximately tenfold greater than that of physically adsorbed TA, with  $5 \times 10^5$  TA molecules per  $\mu$ m<sup>2</sup> (Fig. 2D) [32]. This high grafting density is crucial for achieving high adsorption capacity, offering a large number of binding

# 3.2. Light-enhanced adsorption of selective metal ions

Our investigation accessed the capability of *p*-silica-TA to selectively adsorb precious metal ions from an acidic solution, representing a simulated E-waste scenario, containing a mixture of nine different metal ions. The predominant species in the acidic mixture (0.1 M HCl) included AuCl<sub>4</sub>, PtCl<sub>6</sub><sup>2</sup>, PdCl<sub>2</sub><sup>2</sup>, Cu<sup>2+</sup>, Co<sup>2+</sup>, Ni<sup>2+</sup>, Zn<sup>2+</sup>, Fe<sup>3+</sup>, and Al<sup>3+</sup> ions [43]. These species were identified via their characteristic absorption peaks in the UV-visible spectra, indicative of ligand-to-metal charge transfer (LMCT) events (Fig. S3). Adsorption experiments were performed at metal ion concentrations of 0.1, 1, and 2 mM, corresponding to concentration ranges previously reported for Au (7-350 ppm), Pt (5-33 ppm), and Pd (4-210 ppm) found in E-waste (Table S1). Additionally, the adsorption experiments were conducted both in the dark and under AM1.5-simulated sunlight, and the adsorption efficiency was quantified using inductively coupled plasma optical emission spectrometry (ICP-OES). Notably, p-silica-TA demonstrated a selective and marked affinity for Au, Pt, and Pd ions, with a particularly strong inclination towards Au across all tested concentrations (Fig. 3A and Table S3). For instance, at a concentration of 0.1 mM, the adsorption efficiencies for Au, Pt, and Pd were 99.4 %, 62.6 %, and 62.4 % respectively, in the dark. Note that p-silica-TA effectively captured precious metal ions at concentrations as low as approximately 20, 12, and 6 ppm for Au, Pt, and Pd, respectively, which are close to the lower thresholds found in E-waste compositions [2,20,44]. The observed selectivity and sensitivity may be due to the high reduction potentials of these metals, which facilitate chelation and subsequent reduction by gallol and catechol groups [31,32,45]. Comparative analyses with psilica and p-silica-NH<sub>2</sub>, serving as controls, revealed negligible metal ion adsorption for p-silica, while p-silica-NH2 exhibited significantly reduced capacities for Au, Pt, and Pd uptake, regardless of light exposure (Figs. S4 and S5). Despite the prevalent use of surface functionalization with amines for metal ion adsorption, our findings distinctly demonstrate the superior efficiency of TA-functionalization for retrieving

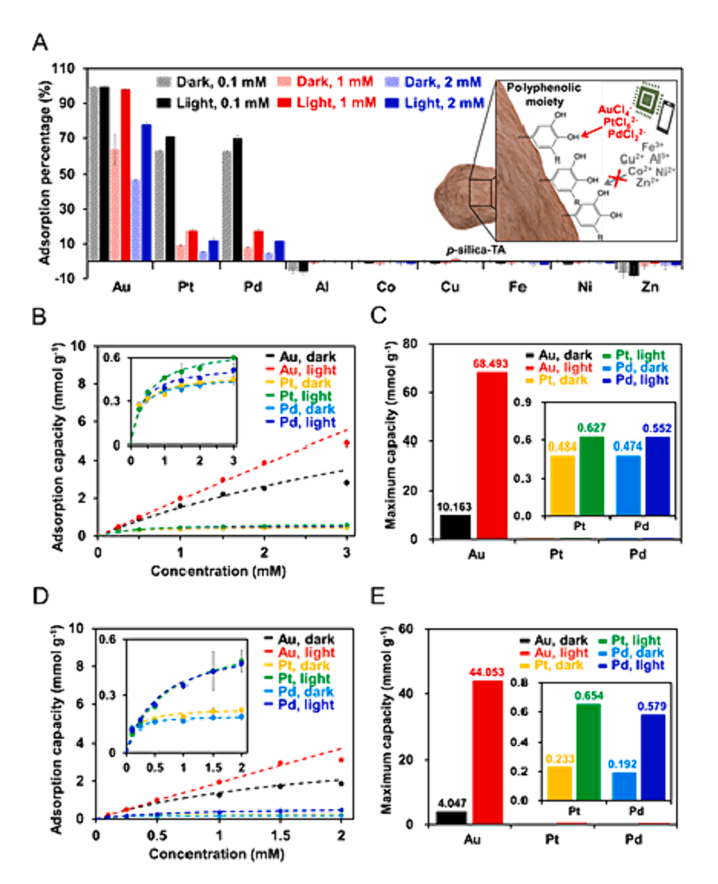


Fig. 3. (A) Adsorption percentages of p-silica-TA for the multi-metal adsorption at concentrations of 0.1, 1, and 2 mM with and without light illumination (inset: illustration for the selective capture of Au, Pt, and Pd ions on p-silica-TA, R = OH or ester). (B) Adsorption isotherms of Au, Pt, and Pd ions in the single-metal adsorption experiments (points: experimental results, dashed line: curves fitted to Langmuir and Freundlich isotherm, inset: magnified spectra). (C) Maximum adsorption capacities determined by the Langmuir isotherms in the single-metal adsorption. (D) Adsorption isotherms of Au, Pt, and Pd ions in the tri-metal adsorption experiments (points: experimental results, dashed line: curves fitted to Langmuir and Freundlich isotherm, inset: magnified spectra). (E) Maximum adsorption capacities determined by the Langmuir isotherms in the tri-metal adsorption.

precious metals from mixed ion solutions [34,46,47]. Control experiments, conducted without any adsorbents, showed only a marginal change ( $\sim$ 5%) in metal ion concentrations, confirming the stability of the metal mixture during the adsorption process (Fig. S6).

Intriguingly, we observed a significant increase in the selective adsorption of Au, Pt, and Pd ions at concentrations of 1 and 2 mM. Specifically, the adsorption efficiencies for Pt and Pd doubled under illumination, although this effect was not pronounced at 0.1 mM. Although most of the added Au ions were already adsorbed on p-silica-TA in the dark, there was a substantial potential for enhancement of the adsorption of Pt and Pd ions. This light-enhanced adsorption can be attributed to the photooxidation of light-sensitive TA, which likely promotes the photodecomposition of precious metal chloro-complexes via LMCT, as demonstrated in our previous report [32]. However, it remains unclear why the enhancement effect was more prominent at higher metal ion concentrations. If TA solely drives the photochemical enhancement, we would expect a greater effect at lower metal ion concentrations, where the TA-to-metal ion ratio is higher, facilitating the adsorption process for Pt and Pd. Yet, the results contradicted our expectations. To address this issue, we hypothesize that the light-driven enhancement is related to the generation of plasmon-induced hot electrons through localized surface plasmon resonance (LSPR) from precious metal nanoparticles. This will be discussed in the next section of this

paper along with results from adsorption isotherms.

# 3.3. Adsorption isotherms of precious metal ions on p-silica-TA

Next, we determined the adsorption isotherms of p-silica-TA for Au, Pt, and Pd ions in acidic aqueous solutions with and without simulated sunlight. This analysis was aimed at exploring the applicability of p-silica-TA as adsorbents across diverse types of E-waste, which may contain single or multiple precious metal ions. The adsorptive capacities  $(q, \text{ in mmol g}^{-1})$  were determined as a function of concentration (C, in mM) of metal ions using ICP-OES, with comprehensive methodologies detailed in Supplementary Data. To elucidate the adsorption mechanisms, Langmuir and Freundlich isotherm models were employed to determine key adsorption parameters with correlation coefficients  $(R^2)$  (Figs. S7-S10 and Table S4-S9).

For the adsorption of individual Au, Pt, and Pd, the Langmuir isotherm model, which predicts monolayer adsorption on a homogenous surface, provided the best fit as indicated by the highest R<sup>2</sup> values, both with and without light irradiation (Fig. 3B and Table S5). Interestingly, Au adsorption under illumination also conformed to the Freundlich isotherm model, suggesting multilayer adsorption on heterogeneous surfaces (Table S6). These findings suggest that while all three precious metals exhibit monolayer adsorption on p-silica-TA, Au uniquely demonstrate multilayer adsorption when exposed to light. In the Langmuir model, the theoretical maximum adsorption capacity  $(q_{max})$ revealed a remarkable increase for Au under sunlight by approximately 6.7-fold (Fig. 3C and Table S5). However, the  $q_{max}$  for Pt and Pd showed modest increases of 1.4 and 1.2-fold, respectively. The  $q_{max}$  for Au under light illumination was an impressive 68.493 mmol g<sup>-1</sup>, appreciably surpassing the capacities of other reported adsorbents [43,48,49]. This contrasted with the dark condition  $q_{max}$  for Au, 10.163 mmol  $g^{-1}$ , comparable to the highest values previously reported (Table S2). However, the  $q_{max}$  values for Pt and Pd under illumination, 0.627 and 0.552 mmol g<sup>-1</sup>, respectively, were similar to those for other adsorbents previously studied [50-54].

In the dark, the adsorption of Au, Pt, and Pd in a tri-metal mixture was well fitted to the Langmuir isotherm (Fig. 3D and Table S8). However, under light illumination, the Freundlich isotherm provided a better fit, analogous to the single-metal adsorption of Au, indicating the diversification of adsorptive sites with varied affinities (Fig. 3E and Table S9). This change can be attributed to the photoexcitation of precious metal species through LMCT, which alters the states of metal species in solution and influences their adsorption potentials with TA. However, the monolayer nature of TA functionalization does not fully explain the metal adsorption behavior in accordance with the Freundlich model. An additional mechanism could be at play, possibly involving the adsorption of metal ions onto pre-existing metal-TA complexes. In particular, under solar irradiation, precious metal ions bound to the gallol and catechol groups of TA can be reduced into metal nanoparticles (MNPs) by the sufficient reduction potential of TA.

As mentioned earlier, plasmon-driven hot electrons are believed to generate heterogeneous adsorption sites by catalyzing the reduction of metal ions into MNPs, which then accumulate into multilayers. It's noteworthy that sunlight raised the  $q_{max}$  values for Au, Pt, and Pd by factors of 11, 2.6, and 3.0, respectively, compared to the increments observed in the single-metal adsorption experiments (Table S8). The noticeable rise of  $q_{max}$  indicates that the light illumination provided photochemical reduction potential, alleviating electrostatic repulsion among precious metal ions. Although the  $q_{max}$  for Au in the tri-metal case (44.053 mmol  $g^{-1}$ ) was lower than in the single-metal scenario (68.493 mmol g<sup>-1</sup>) under sunlight, it still exceeded the capacities reported for other adsorbents (Table S1). In particular, the relative increases in  $q_{max}$  for Pt and Pd by illumination in the tri-metal adsorption were higher than those seen in single-metal adsorptions, revealing the role of plasmon-induced electrons in enhancing the capture of Pt and Pd. Such an effect, previously unreported, underscores the significance of studying adsorption behaviors in mixed solutions of these metal ions. Our findings suggest that the adsorption capacities of *p*-silica-TA for precious metal ions remain robust in mixed ion environments, comparable to in individual ones. Although co-adsorption in the dark may diminish individual metal ion capacities, the presence of plasmonic hot electrons substantially bolsters the simultaneous adsorption of multiple metal ions.

In summary, the selective enhancement of Au, Pt, and Pd ion adsorption on *p*-silica-TA be attributed to two distinct pathways: TA-directed spontaneous reduction of these ions via phenol-to-quinone oxidation, and plasmon-directed reduction by hot electrons generated on MNP surfaces (Fig. 4A). These pathways preferentially adsorb Au, Pt, and Pd ions over other metals, including Cu<sup>2+</sup>, Fe<sup>3+</sup>, Ni<sup>2+</sup>, Co<sup>2+</sup>, Zn<sup>3+</sup>, and Al<sup>3+</sup>, due to their higher reduction potentials compared to the hydroxyl phenolic groups of TA (Fig. 4B) [55–58]. Furthermore, when illuminated, plasmon-induced hot electrons can provide additional reduction potential for metal ions, while plasmonic holes can participate in the oxidation of water and chloride ions [59–61].

# 3.4. Characterization of captured precious metals

Metal-adsorbed p-silica-TA obtained from the tri-metal adsorption is referred to as 'M-p-silica-TA,' where 'M' represents the respective metals: Au, Pt, and Pd. Similarly, particles from single-metal adsorption are denoted as 'Au-p-silica-TA,' 'Pt-p-silica-TA,' and 'Pd-p-silica-TA.' Backscattered electron-SEM (BSE-SEM) and TEM images revealed that illumination markedly increased the formation of MNPs compared to dark conditions, as evidenced by the quantity and size of MNPs (Fig. 5A, 5B, and S11A-D). This phenomenon is attributed to the enhanced reduction of the metal ions and the growth of MNPs. Energy-dispersive X-ray spectroscopy (EDS) with SEM confirmed the simultaneous presence of Au, Pt, and Pd in the M-p-silica-TA, as expected from the ICP-OES results (Fig. S11E). Further, high-angle annular dark-field (HAADF) imaging and EDX elemental mapping in scanning transmission electron microscopy (STEM) analyses revealed the co-localization of Au, Pt, and Pd within the MNPs. Moreover, Pd was observed to form coordination complexes with TA on the p-silica-TA surface (Fig. S12).

Moreover, UV-vis absorption spectra (Fig. 5C) of M-p-silica-TA showed an augmented absorption in the UV and visible regions,

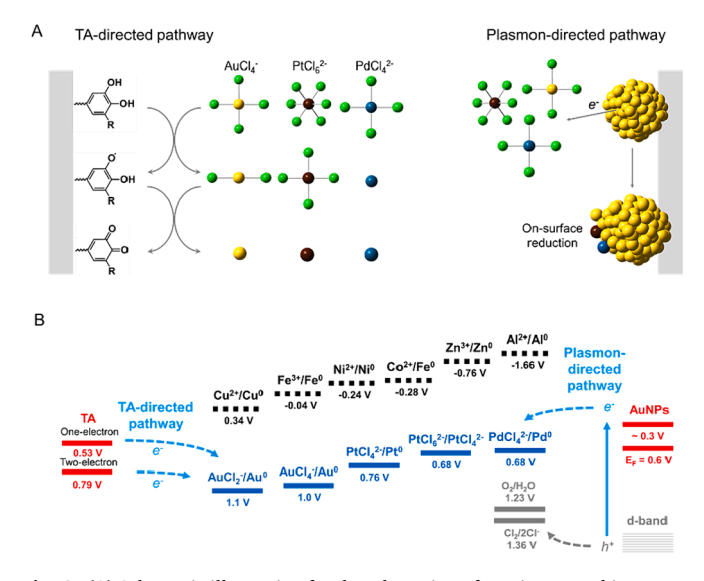


**Fig. 4.** (A) Schematic illustration for the adsorption of precious metal ions on *p*-silica-TA via spontaneous and photochemical reduction by TA-directed and plasmon-directed pathways (colors of atoms: yellow for gold, brown for platinum, blue-green for palladium, and yellow-green for chlorine). (B) Energy diagram representing the standard reduction potentials of TA and metal ions and the energy levels of plasmon-induced charges on AuNPs.

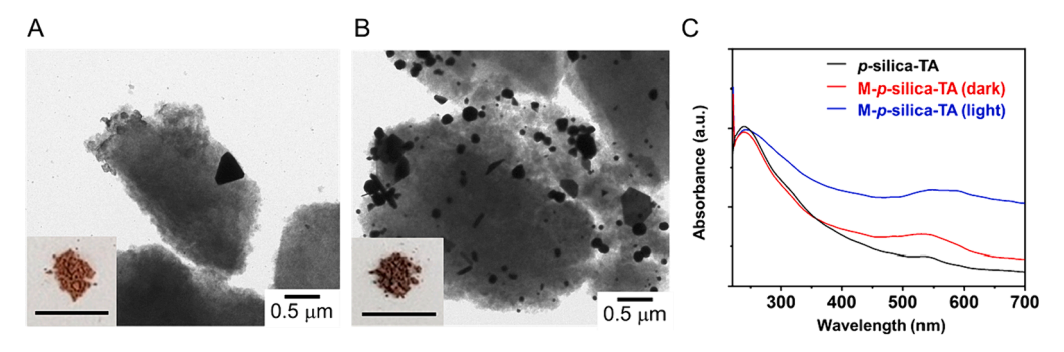


**Fig. 5.** TEM images of M-p-silica-TA without (A) and with (B) light illumination (inset: optical photographs for powders of M-p-silica-TA showing a darker reddish brown color for M-p-silica-TA with light, scale bar: 2 cm). (C) UV-vis absorption spectra of p-silica-TA and M-p-silica-TA dispersed in deionized water using an integrating sphere.

attributed to LSPR of the precious MNPs as supported by previous literatures [62-64]. Particularly, this finding of LSPR can be supplemented by the results of our previous study on Au ion adsorption using TA under different light conditions [32]. It was noted that under visible light, Au ions were predominantly reduced on the surface of Au MNPs via hot electrons generated by LSPR. This process resulted in the growth of Au MNPs, forming sparsely distributed large-sized nanoparticles (183.36  $\pm$ 59.8 nm). Conversely, under ultraviolet light, the tannin-mediated photoreduction of Au ions led to more vigorous nucleation of Au atoms rather than the Au MNPs growth, yielding densely populated smaller-sized nanoparticles (111.7  $\pm$  21.1 nm). The successful adsorption of Au, Pt, and Pd ions by p-silica-TA was also corroborated by the diminished peak intensities corresponding to the precious metal chlorocomplexes in the UV-visible spectra of the remaining solutions (AuCl4 peaks at 226 and 314 nm;  $PtCl_6^{2-}$  peak at 262 nm; and  $PdCl_4^{2-}$  peaks at 224 and 282 nm) (Fig. S13B-D). These metal chloro-complexes are decomposed into reduced intermediates and chlorine ions upon photoexcitation through LMCT, a mechanism akin to the synthesis of MNPs in previous studies [65–72].

FT-IR spectra of M-p-silica-TA showed a notable absence of peaks associated with phenolic O-H bending in the 1380-1310 cm<sup>-1</sup> range, in contrast to p-silica-TA (Fig. S14A). Additionally, an increase in the peak (1650 cm $^{-1}$ ) representing the stretching vibration of C = O in quinone was observed in M-p-silica-TA compared to p-silica-TA, as previously reported [73]. These results suggest that phenolic hydroxyl groups were converted to quinones by participating in the chelation and reduction of metal ions. X-ray powder diffraction (XRD) patterns for M-p-silica-TA displayed distinct peaks at  $2\theta = 38.2, 44.4, 64.6, 77.6,$ and 81.7degrees, indicating the presence of either single-metallic or alloy species of Au, Pt, and Pd (Fig. S14B). The intensified diffraction peaks confirmed that illumination increased the formation of these metallic species. XP survey spectra further confirmed the presence of Au, Pt, and Pd core levels, with peaks for Au 4f, Pt 4f, Pd 3d, Au 4d, and Pt 4d regions observed in both single-metal and tri-metal adsorption cases (Fig. S15). The chemical states of the metals were detailed through peak deconvolution: Au 4f<sub>7/2</sub> (Au  $4f_{5/2}$ ) peak for Au<sup>0</sup> at 84.27 eV (87.97 eV), Pt  $4f_{7/2}$  (Pt  $4f_{5/2}$ ) peak for  $Pt^{0}$  at 71.4 eV (74.75 eV), and Pd  $3d_{5/2}$  (Pd  $3d_{3/2}$ ) peak for  $Pd^{0}$  at 335.3 eV (340.56 eV) (Fig. 6A-C). Alloy formation was inferred from the negative shifts in binding energies (-0.13, -0.3, and -0.3 eV for Au 4f, Pt 4f, and Pd 3d levels, respectively) in M-p-silica-TA from the trimetal adsorption compared to the single-metal case, consistent with previous studies on Au, Pt, and Pd alloys [74-79]. These binding energy shifts resulted from the altered valence levels of the precious metals due to lattice strain and electronic interactions among Au, Pt, and Pd atoms. Atomic percentages of metal species, depicted in Fig. 6D, showed an increase in the ratios of the reduced to oxidized states under light, particularly in the tri-metal adsorption. The higher proportion of reduced metal states is likely due to the synergistic effect of plasmongenerated hot electrons from the MNPs and the photooxidation of TA,

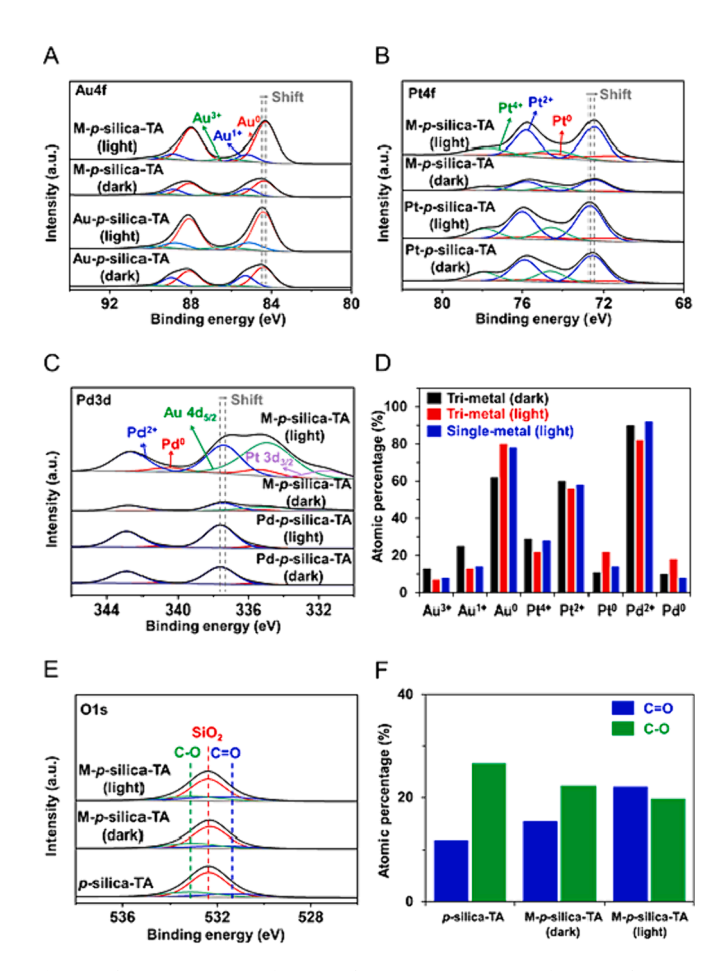


**Fig. 6.** Characterizations of M-p-silica-TA. XP spectra of M-p-silica-TA, Au-p-silica-TA, Pt-p-silica-TA, and Pd-p-silica-TA obtained from the single-metal and tri-metal adsorption in the dark and under light illumination: Au 4f (A), Pt 4f (B), and Pd 3d (C). (D) Atomic percentages of recovered precious metal species on p-silica-TA. (E) XPS spectra for O 1 s regions before and after the adsorption of precious metals (inset: atomic percentage of C-O and C = O species).

which collectively enhance the metal ion reduction process [32].

XPS analysis of O 1 s provided evidence for the photooxidation of TA. The O 1 s spectra were deconvoluted to identify peaks corresponding to carbonyl (C = O) at 531.7 eV and hydroxyl (C-O) species at 533.0 eV, both before and after tri-metal adsorption, as shown in Fig. 6E. A notable increase in the atomic percentage ratio of C = O to C-O species was observed post adsorption: 0.69 in the dark and 1.12 under light exposure. This increase indicates the conversion of the gallol and catechol

groups of TA into quinones, driven by UV light-induced photooxidation (Fig. 6E, inset). Additionally, the presence of chlorine in the XP spectra of M-p-silica—TA suggests the retention of some Au, Pt, and Pd ions in their chloro-complexed forms (Fig. S16).

Our research elucidates the mechanisms underpinning the binding and reduction of Au, Pt, and Pd ions on p-silica-TA, processes that are visibly enhanced under light illumination, as depicted in Fig. 7. Following adsorption, the photooxidation of TA accelerates the reduction of these ions to their atomic states. These metal atoms subsequently aggregate into clusters, which serve as nucleation sites, eventually growing into MNPs. This nucleation and growth of these clusters, particularly the enhancement of their surface area via the Finke-Watzky mechanism, are augmented by the reduction of metal ions on MNPs through the action of plasmon-induced hot electrons [80-82]. Light irradiation thus leads to a greater proportion of reduced metal species, an increased quinone-to-catechol ratio, and the formation of more substantial and numerous MNPs. These growth dynamics contribute to the formation of multilayer structures, consistent with the multilayer adsorption patterns described by the Freundlich isotherm, as shown in Fig. 3.

# 3.5. Metal desorption from M-p-silica-TA

We explored precious metal recovery by two different methods: aqua regia and thiourea leaching, aming to desorb Au, Pt, and Pd from M-p-silica—TA. Aqua regia, known for its rapid dissolution of precious metals, is limited in practical use due to its oxidative and corrosive properties [83–85]. In aqua regia leaching, metallic Au, Pt, and Pd are dissolved into anionic chloride complexes through the action of a potent oxidizing agent (NO $_3$ ) (reactions 1–4) [86].

$$M^{0}(s) + nNO_{3}(aq) + 4nH^{+}(aq) = M^{n+}(aq) + nNO(g) + 2nH_{2}O(l)$$
 (M = Au, Pt, and Pd)(1)

$$Au^{0}(s) + HNO_{3}(aq) + 4HCl(aq) = [AuCl_{4}]^{-}(aq) + NO(g) + H^{+}(aq) + 2H_{2}O(l)(2)$$

$$3Pt^{0}(s) + 4HNO_{3}(aq) + 18HCl(aq) = 3[PtCl_{6}]^{2-}(aq) + 4NO(g) + 6H^{+}(aq) + 8H_{2}O(l)(3)$$

$$3Pd^{0}(s) + 2HNO_{3}(aq) + 12HCl(aq) = 3[PtCl_{4}]^{2}(aq) + 2NO(g) + 6H^{+}(aq) + 4H_{2}O(l)(4)$$

Our results confirmed efficient recovery via aqua regia, with desorption rates of 96.4 %, 96.1 %, and 99.3 % for Au, Pt, and Pd, respectively, as verified by ICP-OES (Fig. 8A). Subsequent analysis with

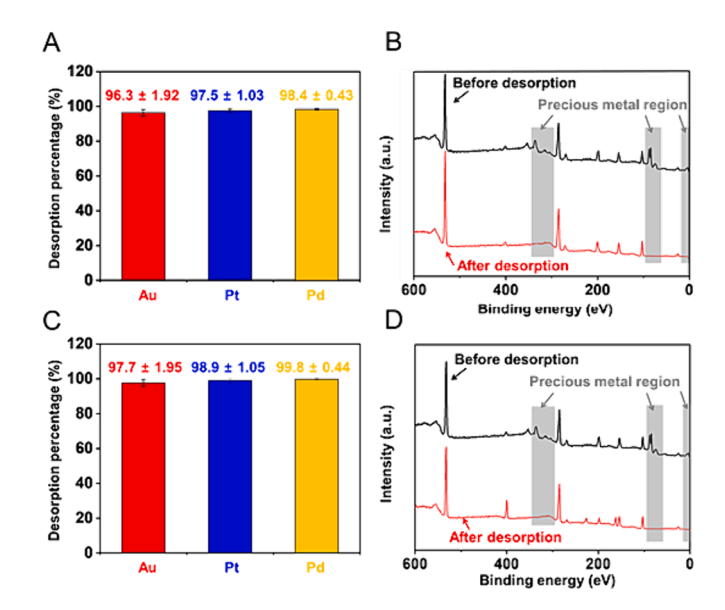


**Fig. 8.** (A) Desorption percentages from aqua regia leaching. (B) XP survey spectra before and after desorption of metals by aqua regia leaching. (C) Desorption percentages from thiourea leaching. (D) XP survey spectra before and after desorption of metals by thiourea leaching.

BSE-SEM and EDS confirmed the removal of these metals from M-p-silica—TA (Fig. S17). XPS analysis revealed the presence of residual ionic species of Au and Pt after leaching, evidenced by low-intensity peaks in the Au 4f, Pt 4f, and Pd 3d spectra, without detectable metallic species (Fig. 8B and S18). These residual chlorocomplexes likely persisted due to electrostatic interactions with the protonated amine groups on the substrate.

Next, we carried out metal ion leaching using an acidic thiourea solution, a method gaining favor for industrial use [83]. Metallic Au, Pt, and Pd are dissolved into cationic complexes with thiourea in an acidic solution (reactions 5–7) [87–89].

$$\begin{split} &Au^{0}\left(s\right)+2CS(NH_{2})_{2}\left(aq\right)=\left[CS(SC(NH_{2})_{2})_{2}\right]^{+}\left(aq\right)+e^{-}(5)\\ &Pt^{0}\left(s\right)+2CS(NH_{2})_{2}\left(aq\right)=\left[Pt(CS(NH_{2})_{2})_{2}\right]^{4+}\left(aq\right)+e^{4-}(6)\\ &Pd^{0}\left(s\right)+4CS(NH_{2})_{2}\left(aq\right)=\left[Pd(CS(NH_{2})_{2})_{4}\right]^{2+}\left(aq\right)+e^{2-}(7) \end{split}$$

Thiourea leaching yielded even higher desorption efficiencies: 97.7 % for Au, 98.9 % for Pt, and 99.8 % for Pd (Fig. 8C). The effectiveness of

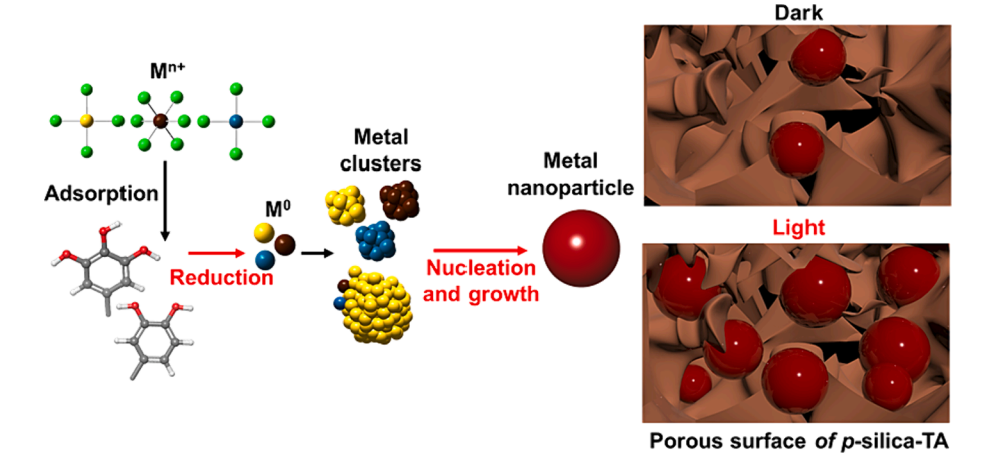


**Fig. 7.** Schematic description of the photochemical reductive adsorption of precious metal ions on *p*-silica-TA where the reduction of metal ions and nucleation and growth of metal clusters, indicated by red arrows, can be promoted by light illumination (colors of atoms: yellow for gold, brown for platinum, blue-green for palladium, yellow-green for chlorine, gray for carbon, red for oxygen, and white for hydrogen).

this approach was supported by XPS (Fig. 8D), as well as BSE-SEM and EDS analyses (Fig. S19), indicating the complete removal of precious metal-thiourea complexes, suggesting a clean desorption process. The thiourea-based method not only yielded high metal recovery rates but also proved to be environmentally benign and operationally simpler [81]. Additionally, the thiourea solution is economically advantageous, costing \$3.6 per 100 mL, compared to \$4.6 per 100 mL for aqua regia, for an equivalent volume of adsorbent.

# 4. Conclusions

We demonstrated that the photochemical activation of polyphenolgrafted mesoporous silica particles is a viable strategy for the efficient and selective recovery of precious metals from E-waste. TA-grafted silica particles revealed high selectivity towards Au, Pt, and Pd in the mixture of multiple metal ions found in E-waste and in a wide range of concentrations. Harnessing photon energies by TA photooxidation and plasmonic hot electron transfer increased the maximum adsorption capacities for Au, Pt, and Pd ions by 6.7, 1.4, and 1.2 times, respectively, in single-metal adsorption scenarios. The maximum adsorption capacity for Au was 13.4 g per gram of adsorbents (68.4 mmol  $g^{-1}$ ), which was much higher than the highest values ever reported in the literature (Table S2). The photoactivated TA-grafted silica particles accomplished the increased maximum adsorption capacities by 11, 2.6, and 3 times for Au, Pt, and Pd, respectively, in the tri-metal adsorption despite the competitive adsorption among the metal ions. The exceptionally efficient metal adsorption was photochemically induced in conjunction with the high grafting density of TA. The plasmonic effect also provided sufficient hot electrons to overcome the barriers posed by the limited number of adsorption sites and the competitive adsorption dynamics among different metal ions. Moreover, the acidic thiourea-based leaching process achieved high metal recovery percentages (97.7-99.8 %) from the TA-grafted silica particles capturing precious metals. The advantages of the TA-grafted silica include large adsorption capacity, selectivity towards precious metal ions, eco-friendliness of the materials, and easiness of mass production potentially at a low cost. Overall, the photoinitiated activation of polyphenol-based adsorptive materials offers a practical approach for the urban mining of precious metals from E-waste.

# CRediT authorship contribution statement

Jeonga Kim: Writing – original draft, Visualization, Software, Methodology, Formal analysis, Data curation. Kimoon Lee: Software, Methodology, Formal analysis, Data curation. Cafer T. Yavuz: Validation, Supervision, Formal analysis, Conceptualization. Yoon Sung Nam: Writing – review & editing, Supervision, Project administration, Investigation, Funding acquisition, Formal analysis, Data curation, Conceptualization.

# Declaration of competing interest

The authors declare that they have no known competing financial interests or personal relationships that could have appeared to influence the work reported in this paper.

# Data availability

Data will be made available on request.

# Acknowledgments

This work was financially supported by the Basic Science Research Program and Nano-Material Technology Development Program through the National Research Foundation of Korea (NRF) funded by the the Ministry of Science and ICT (NRF-2020R1A2C2004168 and nrf-

2020r1a2c2004168), Republic of Korea.

# Appendix A. Supplementary material

Supplementary data to this article can be found online at https://doi.org/10.1016/j.cej.2024.150529.

# References

- [1] Y. Chen, Q. Qiao, J. Cao, H. Li, Z. Bian, Precious metal recovery, Joule. 5 (2021) 3097–3115, https://doi.org/10.1016/j.joule.2021.11.002.
- [2] A. Işıldar, E.R. Rene, E.D. van Hullebusch, P.N.L. Lens, Electronic waste as a secondary source of critical metals: management and recovery technologies, Resour. Conserv. Recycl. 135 (2018) 296–312, https://doi.org/10.1016/j. rescourec.2017.07.031.
- J. Cui, L. Zhang, Metallurgical recovery of metals from electronic waste: a review, J. Hazard. Mater. 158 (2008) 228–256, https://doi.org/10.1016/j. ihazmat.2008.02.001.
- [4] E. Hsu, K. Barmak, A.C. West, A.H.A. Park, Advancements in the treatment and processing of electronic waste with sustainability: a review of metal extraction and recovery technologies, Green Chem. 21 (2019) 919–936, https://doi.org/10.1039/ c8gc03688h.
- [5] J.R. Dodson, H.L. Parker, A.M. García, A. Hicken, K. Asemave, T.J. Farmer, H. He, J.H. Clark, A.J. Hunt, Bio-derived materials as a green route for precious & critical metal recovery and re-use, Green Chem. 17 (2015) 1951–1965, https://doi.org/ 10.1039/c4gc02483d.
- [6] N.A. Dogan, Y. Hong, E. Ozdemir, C.T. Yavuz, Nanoporous Polymer microspheres with nitrile and Amidoxime functionalities for gas capture and precious metal recovery from E-waste, ACS Sustain. Chem. Eng. 7 (2019) 123–128, https://doi. org/10.1021/acssuschemeng.8b05490.
- [7] T.S. Nguyen, Y. Hong, N.A. Dogan, C.T. Yavuz, Gold recovery from E-waste by porous porphyrin-phenazine network polymers, Chem. Mater. 32 (2020) 5343–5349, https://doi.org/10.1021/acs.chemmater.0c01734.
- [8] E. Birinci, M. Gülfen, A.O. Aydin, Separation and recovery of palladium(II) from base metal ions by melamine-formaldehyde-thiourea (MFT) chelating resin, Hydrometallurgy. 95 (2009) 15–21, https://doi.org/10.1016/j. hydromet. 2008.04.002
- [9] H. Liu, S. Ning, S. Zhang, X. Wang, L. Chen, T. Fujita, Y. Wei, Preparation of a mesoporous ion-exchange resin for efficient separation of palladium from simulated electroplating wastewater, J. Environ. Chem. Eng. 10 (2022) 106966, https://doi.org/10.1016/j.jece.2021.106966.
- [10] S. Xu, S. Ning, Y. Wang, X. Wang, H. Dong, L. Chen, X. Yin, T. Fujita, Y. Wei, Precise separation and efficient enrichment of palladium from wastewater by amino-functionalized silica adsorbent, J. Clean. Prod. 396 (2023) 136479, https:// doi.org/10.1016/i.iclepro.2023.136479.
- [11] Y. Hong, D. Thirion, S. Subramanian, M. Yoo, H. Choi, H.Y. Kim, J. Fraser Stoddart, C.T. Yavuz, Precious metal recovery from electronic waste by a porous porphyrin polymer, Proc. Natl. Acad. Sci. U.S.A. 117 (2020) 16174–16180, https://doi.org/ 10.1073/pnas.2000606117.
- [12] Y. Hong, V. Rozyyev, C.T. Yavuz, Alkyl-linked porphyrin porous Polymers for gas capture and precious metal adsorption, Small Sci. 1 (2021) 2000078, https://doi. org/10.1002/smsc.202000078.
- [13] M. Garai, M. Mahato, Y. Hong, V. Rozyyev, U. Jeong, Z. Ullah, C.T. Yavuz, Asynchronous double Schiff Base formation of pyrazole porous Polymers for selective pd recovery, Adv. Sci. 8 (2021) 1–10, https://doi.org/10.1002/ advs.202001676.
- [14] T.S. Nguyen, C.T. Yavuz, Selective palladium recovery by a highly porous polyisothiocyanurate, Chem. 8 (2022) 1793–1796, https://doi.org/10.1016/j. chempr.2022.06.009.
- [15] A. Ramesh, H. Hasegawa, W. Sugimoto, T. Maki, K. Ueda, Adsorption of gold(III), platinum(IV) and palladium(II) onto glycine modified crosslinked chitosan resin, Bioresour. Technol. 99 (2008) 3801–3809, https://doi.org/10.1016/j. biortech 2007 07 008
- [16] K. Fujiwara, A. Ramesh, T. Maki, H. Hasegawa, K. Ueda, Adsorption of platinum (IV), palladium (II) and gold (III) from aqueous solutions onto I-lysine modified crosslinked chitosan resin, J. Hazard. Mater. 146 (2007) 39–50, https://doi.org/ 10.1016/j.jhazmat.2006.11.049.
- [17] B. Pangeni, H. Paudyal, M. Abe, K. Inoue, H. Kawakita, K. Ohto, B.B. Adhikari, S. Alam, Selective recovery of gold using some cross-linked polysaccharide gels, Green Chem. 14 (2012) 1917–1927, https://doi.org/10.1039/c2gc35321k.
- [18] B. Pangeni, H. Paudyal, K. Inoue, H. Kawakita, K. Ohto, S. Alam, An assessment of gold recovery processes using cross-linked paper gel, J. Chem. Eng. Data. 57 (2012) 796–804, https://doi.org/10.1021/je201018a.
- [19] M. Kaya, Recovery of metals and nonmetals from electronic waste by physical and chemical recycling processes, Waste Manag. 57 (2016) 64–90, https://doi.org/ 10.1016/j.wasman.2016.08.004.
- [20] Z. Sun, H. Cao, Y. Xiao, J. Sietsma, W. Jin, H. Agterhuis, Y. Yang, Toward sustainability for recovery of critical metals from electronic waste: the hydrochemistry processes, ACS Sustain. Chem. Eng. 5 (2017) 21–40, https://doi. org/10.1021/acssuschemeng.6b00841.
- [21] C.A. Hong, H.Y. Son, Y.S. Nam, Layer-by-layer siRNA/poly(L-lysine) multilayers on polydopamine-coated surface for efficient cell adhesion and gene silencing, Sci. Rep. 8 (2018) 7738, https://doi.org/10.1038/s41598-018-25655-7.

- [22] H.Y. Son, H. Jun, K.R. Kim, C.A. Hong, Y.S. Nam, Tannin-mediated assembly of gold-titanium oxide hybrid nanoparticles for plasmonic photochemical applications, J. Ind. Eng. Chem. 63 (2018) 420–425, https://doi.org/10.1016/j. iiec. 2018.03.002
- [23] J. Kim, K. Lee, Y.S. Nam, Metal-polyphenol complexes as versatile building blocks for functional biomaterials, biotechnol, Bioprocess Eng. 26 (2021) 689–707, https://doi.org/10.1007/S12257-021-0022-4.
- [24] H.Y. Son, B. Il Koo, J.B. Lee, K.R. Kim, W. Kim, J. Jang, M.S. Yoon, J.W. Cho, Y. S. Nam, Tannin-titanium oxide multilayer as a photochemically suppressed ultraviolet filter, ACS Appl. Mater. Interfaces. 10 (2018) 27344–27354, https://doi.org/10.1021/acsami.8b09200.
- [25] S. Choi, J. Kim, R.T. Rahman, D.J. Lee, K. Lee, Y.S. Nam, Plastic-free silica-titaniapolyphenol heterojunction hybrids for efficient UV-to-blue light blocking and suppressed photochemical reactivity, Chem. Eng. J. 431 (2022) 133790, https:// doi.org/10.1016/i.cei.2021.133790.
- [26] I. Kim, N. Jo, Y. Gu, Y.S. Nam, Interstitial polydopamine layer stabilizing catalysts/ electrode interface for sustainable water oxidation, Colloids Surfaces A Physicochem. Eng. Asp. 614 (2021) 126121, https://doi.org/10.1016/j. colsurfa.2020.126121.
- [27] K.R. Kim, J. Kim, J.W. Kim, C.T. Yavuz, M.Y. Yang, Y.S. Nam, Light-activated polydopamine coatings for efficient metal recovery from electronic waste, Sep. Purif. Technol. 254 (2021) 117674, https://doi.org/10.1016/j. seppur 2020 117674
- [28] H.Y. Son, I. Kim, Y.S. Nam, On-surface synthesis of metal nanostructures on solid and hydrated polymer nanofibers coated with polydopamine, J. Ind. Eng. Chem. 30 (2015) 220–224, https://doi.org/10.1016/j.jiec.2015.05.025.
- [29] H.Y. Son, J.H. Nyu, H. Lee, Y.S. Nam, Silver-polydopamine hybrid coatings of electrospun poly(vinyl alcohol) nanofibers, Macromol. Mater. Eng. 298 (2013) 547–554, https://doi.org/10.1002/mame.201200231.
- [30] I. You, S.M. Kang, S. Lee, Y.O. Cho, J.B. Kim, S.B. Lee, Y.S. Nam, H. Lee, Polydopamine microfluidic system toward a two-dimensional, gravity-driven mixing Device, Angew. Chemie - Int. Ed. 51 (2012) 6126–6130, https://doi.org/ 10.1002/anie.201200329.
- [31] K.R. Kim, S. Choi, C.T. Yavuz, Y.S. Nam, Direct Z-scheme tannin-TiO2 heterostructure for photocatalytic gold ion recovery from electronic waste, ACS Sustain. Chem. Eng. 8 (2020) 7359–7370, https://doi.org/10.1021/ acssuschemeng.0c00860.
- [32] J. Kim, K.R. Kim, Y. Hong, S. Choi, C.T. Yavuz, J.W. Kim, Y.S. Nam, Photochemically enhanced selective adsorption of gold ions on tannin-coated porous Polymer microspheres, ACS Appl. Mater. Interfaces. 11 (2019) 21915–21925, https://doi.org/10.1021/acsami.9b05197.
- [33] H.I. Meléndez-Ortiz, Y. Perera-Mercado, J.A. Mercado-Silva, Y. Olivares-Maldonado, G. Castruita, L.A. García-Cerda, Functionalization with amine-containing organosilane of mesoporous silica MCM-41 and MCM-48 obtained at room temperature, Ceram. Int. 40 (2014) 9701–9707, https://doi.org/10.1016/J.CERAMINT.2014.02.051.
- [34] M. Vasudevan, P.L. Sakaria, A.S. Bhatt, H.M. Mody, H.C. Bajaj, Effect of concentration of aminopropyl groups on the Surface of MCM-41 on adsorption of Cu2+, Ind. Eng. Chem. Res. 50 (2011) 11432–11439, https://doi.org/10.1021/ ie2014480
- [35] M.R. Mello, D. Phanon, G.Q. Silveira, P.L. Llewellyn, C.M. Ronconi, Amine-modified MCM-41 mesoporous silica for carbon dioxide capture, Microporous Mesoporous Mater. 143 (2011) 174–179, https://doi.org/10.1016/J.MICROMESO.2011.02.022.
- [36] X. Liu, M. Liang, M. Liu, R. Su, M. Wang, W. Qi, Z. He, Highly efficient catalysis of azo dyes using recyclable silver Nanoparticles immobilized on tannic acid-grafted eggshell membrane, Nanoscale Res. Lett. 11 (2016) 440, https://doi.org/10.1186/ s11671-016-1647-7
- [37] C. Wang, H. Zhou, H. Niu, X. Ma, Y. Yuan, H. Hong, C. Liu, Tannic acid-loaded mesoporous silica for rapid hemostasis and antibacterial activity, Biomater. Sci. 6 (2018) 3318–3331, https://doi.org/10.1039/C8BM00837J.
- [38] S.A. Centeno, J. Shamir, Surface enhanced raman scattering (SERS) and FTIR characterization of the sepia melanin pigment used in works of art, J. Mol. Struct. 873 (2008) 149–159, https://doi.org/10.1016/j.molstruc.2007.03.026.
- [39] M. Mecozzi, M. Pietroletti, M. Scarpiniti, R. Acquistucci, M.E. Conti, Monitoring of marine mucilage formation in italian seas investigated by infrared spectroscopy and independent component analysis, Environ. Monit. Assess. 184 (2012) 6025–6036, https://doi.org/10.1007/s10661-011-2400-4.
- [40] T.M. Budnyak, A. Gładysz-Płaska, A.V. Strizhak, D. Sternik, I.V. Komarov, M. Majdan, V.A. Tertykh, Imidazole-2yl-phosphonic acid derivative grafted onto mesoporous silica Surface as a novel highly effective sorbent for Uranium(VI) ion Extraction, ACS Appl. Mater. Interfaces. 10 (2018) 6681–6693, https://doi.org/ 10.1021/acsami.7b17594.
- [41] S. Palacio, M. Aitkenhead, A. Escudero, G. Montserrat-Martí, M. Maestro, A.H. J. Robertson, Gypsophile chemistry unveiled: fourier transform Infrared (FTIR) spectroscopy provides new insight into plant adaptations to gypsum soils, PLoS One. 9 (2014), https://doi.org/10.1371/journal.pone.0107285.
- [42] D.L. Franco, A.S. Afonso, S.N. Vieira, L.F. Ferreira, R.A. Gonçalves, A.G. Brito-Madurro, J.M. Madurro, Electropolymerization of 3-aminophenol on carbon graphite surface: electric and morphologic properties, Mater. Chem. Phys. 107 (2008) 404–409, https://doi.org/10.1016/j.matchemphys.2007.08.006.
- [43] S. Lin, D.H. Kumar Reddy, J.K. Bediako, M.H. Song, W. Wei, J.A. Kim, Y.S. Yun, Effective adsorption of Pd(II), Pt(IV) and Au(III) by Zr(IV)-based metal-organic frameworks from strongly acidic solutions, J. Mater. Chem. a. 5 (2017) 13557–13564, https://doi.org/10.1039/c7ta02518a.

- [44] L.H. Yamane, V.T. de Moraes, D.C.R. Espinosa, J.A.S. Tenório, Recycling of WEEE: characterization of spent printed circuit boards from mobile phones and computers, Waste Manag. 31 (2011) 2553–2558, https://doi.org/10.1016/j. wasman.2011.07.006.
- [45] T. Ogata, Y. Nakano, Mechanisms of gold recovery from aqueous solutions using a novel tannin gel adsorbent synthesized from natural condensed tannin, Water Res. 39 (2005) 4281–4286, https://doi.org/10.1016/j.watres.2005.06.036.
- [46] K.F. Lam, K.L. Yeung, G. McKay, An investigation of gold adsorption from a Binary mixture with selective mesoporous silica adsorbents, J. Phys. Chem. b. 110 (2006) 2187–2194, https://doi.org/10.1021/jp055577n.
- [47] C.R. Adhikari, D. Parajuli, H. Kawakita, K. Inoue, K. Ohto, H. Harada, Dimethylamine-modified waste paper for the recovery of precious metals, Environ. Sci. Technol. 42 (2008) 5486–5491, https://doi.org/10.1021/es800155x.
- [48] F. Liu, L. Zhou, L. Tao, L. Qian, G. Yu, S. Deng, Adsorption behavior and mechanism of Au(III) on caffeic acid functionalized viscose staple fibers, Chemosphere. 253 (2020) 126704, https://doi.org/10.1016/j. chemosphere.2020.126704.
- [49] X. Chen, Y. Xiang, L. Xu, G. Liu, Recovery and reduction of Au(III) from mixed metal solution by thiourea-resorcinol-formaldehyde microspheres, J. Hazard. Mater. 397 (2020) 122812, https://doi.org/10.1016/j.jhazmat.2020.122812.
- [50] Z. Qin, X. Tang, Y. Su, Z. He, Y. Qu, S. Tong, SnS micro/nanocrystals with urchinlike architectures for capture of Au(III), Pt(IV), and Pd(II), ACS Appl. Nano Mater. 3 (2020) 4102–4113, https://doi.org/10.1021/acsanm.0c00227.
- [51] D. Parajuli, H. Kawakita, K. Inoue, M. Funaoka, Recovery of Gold(III), Palladium (II), and Platinum(IV) by aminated lignin derivatives, Ind. Eng. Chem. Res. 45 (2006) 6405–6412, https://doi.org/10.1021/ie0603518.
- [52] L. Liu, S. Liu, Q. Zhang, C. Li, C. Bao, X. Liu, P. Xiao, Adsorption of Au(III), Pd(II), and Pt(IV) from aqueous solution onto graphene oxide, J. Chem. Eng. Data. 58 (2013) 209–216, https://doi.org/10.1021/je300551c.
- [53] B. Feng, C. Yao, S. Chen, R. Luo, S. Liu, S. Tong, Highly efficient and selective recovery of Au(III) from a complex system by molybdenum disulfide nanoflakes, Chem. Eng. J. 350 (2018) 692–702, https://doi.org/10.1016/j.cej.2018.05.130.
- [54] S. Lin, J.K. Bediako, M.H. Song, J.A. Kim, C.W. Cho, Y. Zhao, J.W. Choi, Y.S. Yun, Effective recovery of Pt(IV) from acidic solution by a defective metal-organic frameworks using central composite design for synthesis, ACS Sustain. Chem. Eng. 7 (2019) 7510–7518, https://doi.org/10.1021/acssuschemeng.8b04637.
- [55] J.C. Danilewicz, Review of oxidative processes in wine and value of reduction potentials in enology, Am. J. Enol. Vitic. 63 (2012) 1–10, https://doi.org/10.5344/ aiev.2011.11046.
- [56] P. Wardman, Reduction potentials of one-electron couples involving free radicals in aqueous solution, J. Phys. Chem. Ref. Data. 18 (1989) 1637–1755, https://doi. org/10.1063/1.555843.
- [57] G. Ziyatdinova, A. Gainetdinova, M. Morozov, H. Budnikov, S. Grazhulene, A. Red'kin, Voltammetric detection of synthetic water-soluble phenolic antioxidants using carbon nanotube based electrodes, J. Solid State Electrochem. 16 (2012) 127–134. https://doi.org/10.1007/510008-011-1295-x.
- [58] H. Wan, Q. Zou, R. Yan, F. Zhao, B. Zeng, Electrochemistry and voltammetric determination of tannic acid on a single-wall carbon nanotube-coated glassy carbon electrode, Microchim. Acta. 159 (2007) 109–115, https://doi.org/10.1007/ 2006.04.006.0717.4
- [59] J.R. Dunklin, A.H. Rose, H. Zhang, E.M. Miller, J. Van De Lagemaat, Plasmonic hot hole transfer in gold Nanoparticle-decorated transition metal dichalcogenide nanosheets, ACS Photonics. 7 (2020) 197–202, https://doi.org/10.1021/ acsphotonics.9b01393.
- [60] C.W. Moon, S.Y. Lee, W. Sohn, D.M. Andoshe, D.H. Kim, K. Hong, H.W. Jang, Plasmonic octahedral gold nanoparticles of maximized near electromagnetic fields for enhancing catalytic hole transfer in solar water splitting, Part. Part. Syst. Charact. 34 (2017) 1600340, https://doi.org/10.1002/ppsc.201600340.
- [61] D.S. Achilleos, H. Kasap, E. Reisner, Photocatalytic hydrogen generation coupled to pollutant utilisation using carbon dots produced from biomass, Green Chem. 22 (2020) 2831–2839, https://doi.org/10.1039/d0gc00318b.
   [62] K.G. Stamplecoskie, P.V. Kamat, Size-dependent excited state behavior of
- [62] K.G. Stamplecoskie, P.V. Kamat, Size-dependent excited state behavior of glutathione-capped gold clusters and their light-Harvesting capacity, J. Am. Chem. Soc. 136 (2014) 11093–11099, https://doi.org/10.1021/ja505361n.
- [63] R.A. Ganeev, M. Suzuki, M. Baba, M. Ichihara, H. Kuroda, Low- and high-order nonlinear optical properties of Au, Pt, Pd, and Ru nanoparticles, J. Appl. Phys. 103 (2008) 063102, https://doi.org/10.1063/1.2887990.
- [64] J.A. Creighton, D.G. Eadon, Ultraviolet-visible absorption spectra of the colloidal metallic elements, J. Chem. Soc. Faraday Trans. 87 (1991) 3881–3891, https://doi. org/10.1039/FT9918703881.
- [65] R.E. Cameron, A.B. Bocarsly, Multielectron-photoinduced reduction of chloroplatinum complexes: visible light deposition of platinum metal, Inorg. Chem. 25 (1986) 2910–2913, https://doi.org/10.1021/ic00236a053.
- [66] R.C. Wright, G.S. Laurence, Production of Platinum(III) by flash photolysis of PtCl62-, J. Chem. Soc. Chem. Commun. (1972) 132–133, https://doi.org/10.1039/ c22720000133
- [67] M. Harada, K. Okamoto, M. Terazima, Diffusion of platinum ions and platinum Nanoparticles during photoreduction processes using the transient grating method, Langmuir. 22 (2006) 9142–9149, https://doi.org/10.1021/la061663i.
- [68] M. Harada, H. Einaga, Formation mechanism of Pt particles by photoreduction of Pt ions in polymer solutions, Langmuir. 22 (2006) 2371–2377, https://doi.org/ 10.1021/Ja052378m.
- [69] S. Eustis, H.Y. Hsu, M.A. El-Sayed, Gold nanoparticle formation from photochemical reduction of Au3+ by continuous excitation in colloidal solutions. a proposed Molecular mechanism, J. Phys. Chem. B 109 (2005) 4811–4815, https:// doi.org/10.1021/jp0441588.

- [70] G. Fan, Y. Han, S. Luo, Y. Li, S. Qu, Q. Wang, R. Gao, M. Chen, M. Han, Mechanism for the photoreduction of poly(vinylpyrrolidone) to HAuCl4 and the dominating saturable absorption of Au colloids, Phys. Chem. Chem. Phys. 18 (2016) 8993–9004, https://doi.org/10.1039/c5cp04382d.
- [71] M. Saeki, T. Taguchi, N. Nakashima, H. Ohba, Wet separation between palladium (II) and molybdenum(IV) ions by using laser-induced particle formation: enhancement of recovery efficiency of palladium by laser condition, J. Photochem. Photobiol. A Chem. 299 (2015) 189–193, https://doi.org/10.1016/j. iphotochem.2014.11.022.
- [72] C. Tian, H. Fang, H. Chen, W. Chen, S. Zhou, X. Duan, X. Liu, Y. Yuan, Photodeposition of Pd onto TiO2 nanowires for aqueous-phase selective hydrogenation of phenolics to cyclohexanones, Nanoscale. 12 (2020) 2603–2612, https://doi.org/10.1039/c9nr08324c.
- [73] Q. Zhao, W. Huang, Z. Luo, L. Liu, Y. Lu, Y. Li, L. Li, J. Hu, H. Ma, J. Chen, High-capacity aqueous zinc batteries using sustainable quinone electrodes, Sci. Adv. 4 (2018), https://doi.org/10.1126/sciadv.aao1761.
- [74] T.S. Chou, M.L. Perlman, R.E. Watson, Electronegativity and electron binding in gold alloys, Phys. Rev. B 14 (1976) 3248–3250, https://doi.org/10.1103/ PhysPayB 14 3248
- [75] P.A.P. Nascente, S.G.C. De Castro, R. Landers, G.G. Kleiman, X-ray photoemission and auger energy shifts in some gold-palladium alloys, Phys. Rev. B 43 (1991) 4659–4666, https://doi.org/10.1103/PhysRevB.43.4659.
- [76] G. Yang, D. Chen, P. Lv, X. Kong, Y. Sun, Z. Wang, Z. Yuan, H. Liu, J. Yang, Coreshell Au-Pd nanoparticles as cathode catalysts for microbial fuel cell applications, Sci. Rep. 6 (2016) 1–9, https://doi.org/10.1038/srep35252.
- [77] D. Chen, J. Li, P. Cui, H. Liu, J. Yang, Gold-catalyzed formation of core-shell gold-palladium nanoparticles with palladium shells up to three atomic layers, J. Mater. Chem. A 4 (2016) 3813–3821, https://doi.org/10.1039/c5ta10303g.
- [78] J. Fan, K. Qi, L. Zhang, H. Zhang, S. Yu, X. Cui, Engineering Pt/Pd interfacial electronic structures for highly efficient hydrogen evolution and alcohol oxidation, ACS Appl. Mater. Interfaces. 9 (2017) 18008–18014, https://doi.org/10.1021/ acsami 7b05290
- [79] D. Wang, X. Cui, Q. Xiao, Y. Hu, Z. Wang, Y.M. Yiu, T.K. Sham, Electronic behaviour of Au-Pt alloys and the 4f binding energy shift anomaly in Au bimetallics- X-ray spectroscopy studies, AIP Adv. 8 (2018) 065210, https://doi. org/10.1063/1.5027251.

- [80] N.T.K. Thanh, N. Maclean, S. Mahiddine, Mechanisms of nucleation and growth of Nanoparticles in solution, Chem. Rev. 114 (2014) 7610–7630, https://doi.org/ 10.1021/cr400544s
- [81] T.H. Yang, H.C. Peng, S. Zhou, C.T. Lee, S. Bao, Y.H. Lee, J.M. Wu, Y. Xia, Toward a quantitative understanding of the reduction pathways of a salt precursor in the synthesis of metal nanocrystals, Nano Lett. 17 (2017) 334–340, https://doi.org/ 10.1021/acs.nanolett.6b04151.
- [82] M. Harada, S. Kizaki, Formation mechanism of gold Nanoparticles synthesized by photoreduction in aqueous ethanol solutions of Polymers using in situ quick scanning X-ray absorption fine structure and small-angle X-ray scattering, Cryst. Growth Des. 16 (2016) 1200–1212, https://doi.org/10.1021/acs.cgd.5b01168.
- [83] L. Jing-ying, X. Xiu-li, L. Wen-quan, Thiourea leaching gold and silver from the printed circuit boards of waste mobile phones, Waste Manag. 32 (2012) 1209–1212, https://doi.org/10.1016/j.wasman.2012.01.026.
- [84] A. Tuncuk, V. Stazi, A. Akcil, E.Y. Yazici, H. Deveci, Aqueous metal recovery techniques from e-scrap: Hydrometallurgy in recycling, Miner. Eng. 25 (2012) 28–37, https://doi.org/10.1016/j.mineng.2011.09.019.
- [85] M. Wang, Q. Tan, J.F. Chiang, J. Li, Recovery of rare and precious metals from urban mines—a review, front, Environ. Sci. Eng. 11 (2017) 1–17, https://doi.org/ 10.1007/s11783-017-0963-1.
- [86] M.Q. Hammadi, R.S. Yassen, K.N. Abid, Recovery of platinum and palladium from scrap automotive catalytic converters, Al-Khwarizmi Eng. J. 13 (2017) 131–141, https://doi.org/10.22153/kej.2017.04.002.
- [87] A. Batnasan, K. Haga, Recovery of precious and base metals from waste printed circuit Boards using a sequential leaching procedure, JOM. 70 (2018) 124–128, https://doi.org/10.1007/s11837-017-2694-y.
- [88] V.T. Nguyen, K. Binnemans, Refining of palladium, platinum, and rhodium from a pregnant leach solution of spent automotive catalysts by continuous countercurrent solvent Extraction with ionic liquids in mixer-settlers, Ind. Eng. Chem. Res. 62 (2023) 9549–9562, https://doi.org/10.1021/acs.iecr.3c00851.
- [89] S.M. Sadeghi, H.M.V.M. Soares, A sustainable hydrometallurgical strategy for recycling efficiently platinum from spent reforming petroleum catalyst, Environ. Sci. Pollut. Res. 30 (2023) 101410–101423, https://doi.org/10.1007/s11356-023-28064.1